



Selectively localized Wannier functions

Runzhi Wang,¹ Emanuel A. Lazar,² Hyowon Park,^{1,3} Andrew J. Millis,¹ and Chris A. Marianetti³

¹*Department of Physics, Columbia University, New York, New York 10027, USA*

²*Materials Science and Engineering, University of Pennsylvania, Philadelphia, Pennsylvania 19104, USA*

³*Applied Physics and Applied Mathematics, Columbia University, New York, New York 10027, USA*

(Received 18 July 2014; revised manuscript received 5 September 2014; published 17 October 2014)

Since the seminal work of Marzari and Vanderbilt, maximally localized Wannier functions have become widely used as a real-space representation of the electronic structure of periodic materials. In this paper we introduce selectively localized Wannier functions which extend the method of Marzari and Vanderbilt in two important ways. First, our method allows us to focus on localizing a subset of orbitals of interest. Second, our method allows us to fix centers of these orbitals, and ensure the preservation of the point-group symmetry. These characteristics are important when Wannier functions are used in methodologies that go beyond density functional theory by treating a local subspace of the Hamiltonian more effectively. Application of our method to GaAs, SrMnO₃, and Co demonstrates that selectively localized Wannier functions can offer improvements over the maximally localized Wannier function technique.

DOI: [10.1103/PhysRevB.90.165125](https://doi.org/10.1103/PhysRevB.90.165125)

PACS number(s): 71.15.Ap

I. INTRODUCTION

Solving the Schrödinger equation in crystalline solids typically relies on the use of the translation group to block-diagonalize the Hamiltonian, yielding Bloch states $\psi_{n\mathbf{k}}$, where \mathbf{k} is a wave vector in the first Brillouin zone of the solid and $n \in \{1, 2, \dots, J\}$ is a band index. However, it is often both physically and computationally desirable to have a real-space, atomic-like representation of the Hamiltonian. An approach to achieve this was introduced by Wannier in 1937 [1]. Considering a single band, Wannier introduced the following transformation:

$$|\mathbf{R}n\rangle = \frac{V}{(2\pi)^3} \int d\mathbf{k} e^{-i\mathbf{k}\cdot\mathbf{R}} |\psi_{n\mathbf{k}}\rangle, \quad (1)$$

so that

$$|\psi_{n\mathbf{k}}\rangle = \sum_{\mathbf{R}} e^{i\mathbf{k}\cdot\mathbf{R}} |\mathbf{R}n\rangle, \quad (2)$$

where \mathbf{R} is any lattice vector and V is the unit cell volume. The function $\langle \mathbf{r} | \mathbf{R}n \rangle$ is referred to as a Wannier function.

Because each Bloch function $\psi_{n\mathbf{k}}$ can be adjusted by an arbitrary phase $e^{i\varphi_{n\mathbf{k}}}$, the Wannier functions are not uniquely defined, and we can rewrite Eq. (1) as

$$|\mathbf{R}n\rangle = \frac{V}{(2\pi)^3} \int d\mathbf{k} e^{-i\mathbf{k}\cdot\mathbf{R}} e^{i\varphi_{n\mathbf{k}}} |\psi_{n\mathbf{k}}\rangle. \quad (3)$$

If Wannier functions are constructed from a set of J bands, there is an even greater freedom, since at each k point we may use an arbitrary unitary transformation of band states. Denoting an arbitrary $J \times J$ unitary matrix as $U^{\mathbf{k}}$, then at a given k point we are free to mix the Bloch states as follows:

$$|\tilde{\psi}_{n\mathbf{k}}\rangle = \sum_{m=1}^J U_{mn}^{\mathbf{k}} |\psi_{m\mathbf{k}}\rangle, \quad (4)$$

by which we can define generalized Wannier functions:

$$|\mathbf{R}n\rangle = \frac{V}{(2\pi)^3} \int d\mathbf{k} e^{-i\mathbf{k}\cdot\mathbf{R}} |\tilde{\psi}_{n\mathbf{k}}\rangle. \quad (5)$$

This “gauge freedom” may be exploited to define Wannier functions that are optimized for particular purposes. One approach, pioneered by Marzari and Vanderbilt [2], is to choose the $U^{\mathbf{k}}$ such that the complete set of Wannier functions are as localized as possible in the position representation. Specifically, if we let

$$\bar{\mathbf{r}}_n = \langle \mathbf{0}n | \mathbf{r} | \mathbf{0}n \rangle \quad (6)$$

and

$$\langle r^2 \rangle_n = \langle \mathbf{0}n | r^2 | \mathbf{0}n \rangle, \quad (7)$$

then we can define the total spread functional Ω of the J Wannier functions $|\mathbf{R}n\rangle$ as

$$\Omega = \sum_{n=1}^J [\langle r^2 \rangle_n - \bar{\mathbf{r}}_n^2] \quad (8)$$

and choose the matrices $U^{\mathbf{k}}$ by minimizing Ω [2]. The functions resulting from this procedure are termed maximally localized Wannier functions (MLWFs). In addition to introducing the MLWF method, Marzari and Vanderbilt introduced a gradient descent method for performing the minimization.

While MLWFs are now very widely used, the global spread function given in Eq. (8) is not necessarily optimal for all uses. In recent years attention has focused on methodologies that go beyond density functional theory (DFT) by more appropriately treating electronic correlations in some relevant local subspace of the Hamiltonian. For example, in the DFT+ U and DFT plus dynamical mean field theory (DMFT) methods one treats beyond DFT correlations in a local subspace corresponding to atomic-like d (for transition metals or transition-metal oxides) or f (for rare-earth or actinide intermetallics) orbitals. In these applications, it is important to have a correct local description of the local subspace, including both the correct location of the centers of the correlated orbitals and the correct point symmetry, but the properties of the other degrees of freedom are irrelevant. The MLWF procedure, which treats all orbitals on an equal footing, may give a suboptimal description of the orbitals of interest and in particular does not guarantee that the centers and point symmetries of the orbitals of interest are

correctly described. It is important to note that the method of Wannier functions for entangled energy bands [3] also does not fulfill these goals. In this paper we develop a technique which allows the selective localization of a subset of Wannier orbitals, with specified Wannier center and point symmetry.

The remainder of this paper is outlined as follows. In Sec. II, we outline our methodology. In Sec. III, we illustrate the utility of our method in the one-dimensional chain. In Sec. IV, we present applications to GaAs, SrMnO₃, and Co. In Sec. V, we analyze the Hamiltonian in the Wannier basis for SrMnO₃ and Co.

II. METHOD

Here we derive all of the relevant equations for our formalism. For simplicity we present a construction in which the total number of Wannier functions is equal to the total number, J , of bands under consideration. We believe that our method can be extended to incorporate the inner and outer window construction of Souza *et al.* [3] but this extension is not attempted in this paper because it does not appear to be necessary for the applications we consider. We formulate the problem using a “band window” construction which in principle requires no assumptions about separation of bands. However, the applications we envisage (for example to DMFT calculations) require a basis set that faithfully represents the charge density. Therefore, it is essential that the lowest included band is separated from lower bands by an energy gap, and in what follows we choose windows such that this is the case.

In the rest of this section we first describe the selective localization of a subset of $J' < J$ orbitals, then we present the procedure for fixing the centers of the localized orbitals and finally explain how we constrain the symmetry of the localized orbitals. In the remainder of the paper we use MLWF to refer to the maximal localization method [2,4], SLWF to refer to the selectively localized Wannier method presented here; SLWF+C refers to the same method with centers fixed; SLWF+CS refers to the same method with both centers and symmetries fixed, as described in Appendix A. Our SLWF method produces two types of Wannier functions: objective Wannier functions (OWFs) which have a minimum cumulative spread and the remaining Wannier functions to which we assign no specific name.

A. Selective localization

We construct a subset of localized orbitals by minimizing the following functional:

$$\Omega = \sum_{n=1}^{J'} [\langle r^2 \rangle_n - \bar{\mathbf{r}}_n^2], \quad (9)$$

where $J' \leq J$ is the number of objective Wannier functions that we choose; recall that J is the total number of Wannier functions, or equivalently the number of bands considered. Our method reduces to MLWF when $J' = J$.

Marzari and Vanderbilt showed [2] that in the case $J' = J$, Ω can be decomposed into the sum of two terms, one of which is invariant under arbitrary unitary transformations. However,

when $J' < J$, this is no longer the case, but the minimization of the functional can still be accomplished by methods very similar to those of Marzari and Vanderbilt.

We write $\Omega = \Omega_{\text{IOD}} + \Omega_D$, where

$$\Omega_{\text{IOD}} = \sum_{n=1}^{J'} \left[\langle r^2 \rangle_n - \sum_{\mathbf{R}} |\langle \mathbf{R}n | \mathbf{r} | \mathbf{0}n \rangle|^2 \right], \quad (10)$$

$$\Omega_D = \sum_{n=1}^{J'} \sum_{\mathbf{R} \neq \mathbf{0}} |\langle \mathbf{R}n | \mathbf{r} | \mathbf{0}n \rangle|^2. \quad (11)$$

Following Ref. [2] we recast the expression as a discretized sum in k space:

$$\Omega_{\text{IOD}} = \frac{1}{N} \sum_{n=1}^{J'} \sum_{\mathbf{k}, \mathbf{b}} w_b (1 - |M_{mn}^{\mathbf{k}, \mathbf{b}}|^2), \quad (12)$$

$$\Omega_D = \frac{1}{N} \sum_{n=1}^{J'} \sum_{\mathbf{k}, \mathbf{b}} w_b (\text{Im} \ln M_{mn}^{\mathbf{k}, \mathbf{b}} + \mathbf{b} \cdot \bar{\mathbf{r}}_n)^2, \quad (13)$$

where $M_{mn}^{\mathbf{k}, \mathbf{b}} \equiv \langle u_{m\mathbf{k}} | u_{n\mathbf{k}+\mathbf{b}} \rangle$, \mathbf{b} are vectors which connect a k point to its near neighbors, and w_b is a weight for each $|\mathbf{b}| = b$ such that $\sum_{\mathbf{b}} w_b b_\alpha b_\beta = \delta_{\alpha\beta}$ (see Appendix B of Ref. [2] for a detailed explanation).

Under the infinitesimal unitary transformation, $U_{mn}^{\mathbf{k}} = \delta_{mn} + dW_{mn}^{\mathbf{k}}$, where $dW^{\mathbf{k}\dagger} = -dW^{\mathbf{k}}$, the wave functions transform as

$$|u_{n\mathbf{k}}\rangle \rightarrow |u_{n\mathbf{k}}\rangle + \sum_{m=1}^J dW_{mn}^{\mathbf{k}} |u_{m\mathbf{k}}\rangle \quad (14)$$

so that

$$d\Omega_{\text{IOD}} = \frac{4}{N} \sum_{\mathbf{k}, \mathbf{b}} w_b \sum_{n=1}^{J'} \sum_{m=1}^J \text{Re} (dW_{nm}^{\mathbf{k}} R_{mn}^{\mathbf{k}, \mathbf{b}}), \quad (15)$$

$$d\Omega_D = -\frac{4}{N} \sum_{\mathbf{k}, \mathbf{b}} w_b \sum_{n=1}^{J'} \sum_{m=1}^J \text{Im} (dW_{nm}^{\mathbf{k}} T_{mn}^{\mathbf{k}, \mathbf{b}}), \quad (16)$$

where

$$R_{mn}^{\mathbf{k}, \mathbf{b}} = M_{mn}^{\mathbf{k}, \mathbf{b}} M_{nn}^{\mathbf{k}, \mathbf{b}*}, \quad (17)$$

$$T_{mn}^{\mathbf{k}, \mathbf{b}} = \tilde{R}_{mn}^{\mathbf{k}, \mathbf{b}} (\text{Im} \ln M_{nn}^{\mathbf{k}, \mathbf{b}} + \mathbf{b} \cdot \bar{\mathbf{r}}_n), \quad (18)$$

$$\tilde{R}_{mn}^{\mathbf{k}, \mathbf{b}} = M_{mn}^{\mathbf{k}, \mathbf{b}} / M_{nn}^{\mathbf{k}, \mathbf{b}}. \quad (19)$$

Thus, the gradient of the spread functional is

$$G_{mn}^{\mathbf{k}} = \frac{d\Omega}{dW_{mn}^{\mathbf{k}}} = \begin{cases} 4 \sum_{\mathbf{b}} w_b (\mathcal{A}[R_{mn}^{\mathbf{k}, \mathbf{b}}] - \mathcal{A}[T_{mn}^{\mathbf{k}, \mathbf{b}}]) & m \leq J', n \leq J', \\ -4 \sum_{\mathbf{b}} w_b \left(\frac{R_{mn}^{\mathbf{k}, \mathbf{b}*}}{2} + \frac{T_{mn}^{\mathbf{k}, \mathbf{b}*}}{2i} \right) & m \leq J', n > J', \\ 4 \sum_{\mathbf{b}} w_b \left(\frac{R_{mn}^{\mathbf{k}, \mathbf{b}}}{2} - \frac{T_{mn}^{\mathbf{k}, \mathbf{b}}}{2i} \right) & m > J', n \leq J', \\ 0 & m > J', n > J', \end{cases} \quad (20)$$

where $\mathcal{A}[R_{mn}^{\mathbf{k},\mathbf{b}}] = (R_{mn}^{\mathbf{k},\mathbf{b}} - R_{nm}^{\mathbf{k},\mathbf{b}*})/2$, $\mathcal{S}[T_{mn}^{\mathbf{k},\mathbf{b}}] = (T_{mn}^{\mathbf{k},\mathbf{b}} + T_{nm}^{\mathbf{k},\mathbf{b}*})/2i$.

Following Ref. [2], we minimize Ω by updating $U^{\mathbf{k}}$ in small steps according to $\exp[dW^{\mathbf{k}}]$, choosing

$$dW^{\mathbf{k}} = \epsilon G^{\mathbf{k}}, \quad (21)$$

where ϵ is a positive infinitesimal. We thus have

$$\begin{aligned} d\Omega &= \sum_{\mathbf{k}} \sum_{m,n=1}^J G_{mn}^{\mathbf{k}} dW_{nm}^{\mathbf{k}} \\ &= -\epsilon \sum_{\mathbf{k}} \sum_{m,n=1}^J |G_{mn}^{\mathbf{k}}|^2, \end{aligned} \quad (22)$$

using the identity $G^\dagger = -G$. Thus, it is guaranteed that $d\Omega \leq 0$. This allows us to iteratively update the unitary matrix until a converged solution is attained. In practice, we fix the step size by choosing $\epsilon = \alpha/4w$, where $w = \sum_{\mathbf{b}} w_{\mathbf{b}}$, and minimize the spread using a nonlinear conjugate gradient method [5]. While this method finds only local minima, we have found in practice that if a reasonable starting point is chosen, physically reasonable minima are found and we believe these are global minima based on substantial testing.

B. Fixing centers

To fix the centers of our objectively localized Wannier functions we introduce a Lagrange multiplier to constrain the Wannier center $\bar{\mathbf{r}}_n$:

$$\lambda_c \sum_{n=1}^{J'} (\bar{\mathbf{r}}_n - \mathbf{r}_{0n})^2, \quad (23)$$

where \mathbf{r}_{0n} is the desired center for the n th Wannier function, and λ_c is a Lagrange multiplier for this constraint. Here J' is chosen to allow for a selective localization. We impose this constraint into Ω which is defined by Eq. (9) and introduce a new target functional:

$$\Omega_c = \sum_{n=1}^{J'} [(r^2)_n - \bar{\mathbf{r}}_n^2 + \lambda_c (\bar{\mathbf{r}}_n - \mathbf{r}_{0n})^2]. \quad (24)$$

We decompose Ω_c in a manner similar to that in the previous subsection, but with an additional term $\Omega_{c,v}$ that results from the imposed constraint:

$$\Omega_c = \Omega_{c,\text{IOD}} + \Omega_{c,D} + \Omega_{c,v}, \quad (25)$$

where

$$\Omega_{c,\text{IOD}} = \sum_{n=1}^{J'} \left[\langle r^2 \rangle_n - (1 - \lambda_c) \sum_{\mathbf{R}} |(\mathbf{R}n|\mathbf{r}|\mathbf{0}n)|^2 \right], \quad (26)$$

$$\Omega_{c,D} = (1 - \lambda_c) \sum_{n=1}^{J'} \sum_{\mathbf{R} \neq \mathbf{0}} |(\mathbf{R}n|\mathbf{r}|\mathbf{0}n)|^2, \quad (27)$$

$$\Omega_{c,v} = \lambda_c \sum_{n=1}^{J'} \mathbf{r}_{0n}^2 - 2\lambda_c \sum_{n=1}^{J'} \mathbf{r}_{0n} \cdot \bar{\mathbf{r}}_n. \quad (28)$$

We can recast the expression as a discretized sum in k space:

$$\Omega_{c,\text{IOD}} = \frac{1}{N} \sum_{n=1}^{J'} \sum_{\mathbf{k},\mathbf{b}} w_{\mathbf{b}} [1 - |M_{nn}^{\mathbf{k},\mathbf{b}}|^2 + \lambda_c (\text{Im} \ln M_{nn}^{\mathbf{k},\mathbf{b}})^2], \quad (29)$$

$$\Omega_{c,D} = (1 - \lambda_c) \frac{1}{N} \sum_{n=1}^{J'} \sum_{\mathbf{k},\mathbf{b}} w_{\mathbf{b}} (\text{Im} \ln M_{nn}^{\mathbf{k},\mathbf{b}} + \mathbf{b} \cdot \bar{\mathbf{r}}_n)^2, \quad (30)$$

$$\Omega_{c,v} = \lambda_c \sum_{n=1}^{J'} \mathbf{r}_{0n}^2 + \lambda_c \frac{2}{N} \sum_{\mathbf{k},\mathbf{b}} w_{\mathbf{b}} \mathbf{b} \cdot \sum_{n=1}^{J'} \mathbf{r}_{0n} \text{Im} \ln M_{nn}^{\mathbf{k},\mathbf{b}}. \quad (31)$$

Under the infinitesimal unitary transformation, we have

$$\begin{aligned} d\Omega_{c,\text{IOD}} &= \frac{4}{N} \sum_{\mathbf{k},\mathbf{b}} w_{\mathbf{b}} \sum_{n=1}^{J'} \sum_{m=1}^J [\text{Re}(dW_{nm}^{\mathbf{k}} R_{mn}^{\mathbf{k},\mathbf{b}}) \\ &\quad - \lambda_c \text{Im} \ln M_{nn}^{\mathbf{k},\mathbf{b}} \text{Im}(dW_{nm}^{\mathbf{k}} \tilde{R}_{mn}^{\mathbf{k},\mathbf{b}})], \end{aligned} \quad (32)$$

$$d\Omega_{c,D} = -(1 - \lambda_c) \frac{4}{N} \sum_{\mathbf{k},\mathbf{b}} w_{\mathbf{b}} \sum_{n=1}^{J'} \sum_{m=1}^J \text{Im}(dW_{nm}^{\mathbf{k}} T_{mn}^{\mathbf{k},\mathbf{b}}), \quad (33)$$

$$d\Omega_{c,v} = -\lambda_c \frac{4}{N} \sum_{\mathbf{k},\mathbf{b}} w_{\mathbf{b}} \mathbf{b} \cdot \sum_{n=1}^{J'} \sum_{m=1}^J \mathbf{r}_{0n} \text{Im}(dW_{nm}^{\mathbf{k}} \tilde{R}_{mn}^{\mathbf{k},\mathbf{b}}). \quad (34)$$

Thus, the gradient of the functional is

$$\begin{aligned} G_{c,mn}^{\mathbf{k}} &= \frac{d\Omega_c}{dW_{nm}^{\mathbf{k}}} \\ &= \begin{cases} 4 \sum_{\mathbf{b}} w_{\mathbf{b}} \{ \mathcal{A}[R_{mn}^{\mathbf{k},\mathbf{b}}] - (1 - \lambda_c) \mathcal{S}[T_{mn}^{\mathbf{k},\mathbf{b}}] \} \\ -4\lambda_c \sum_{\mathbf{b}} w_{\mathbf{b}} \left[\frac{\tilde{R}_{mn}^{\mathbf{k},\mathbf{b}}}{2i} \text{Im} \ln M_{nn}^{\mathbf{k},\mathbf{b}} + \frac{\tilde{R}_{nm}^{\mathbf{k},\mathbf{b}*}}{2i} \text{Im} \ln M_{mm}^{\mathbf{k},\mathbf{b}} + \mathbf{b} \cdot (\mathbf{r}_{0n} \frac{\tilde{R}_{mn}^{\mathbf{k},\mathbf{b}}}{2i} + \mathbf{r}_{0m} \frac{\tilde{R}_{nm}^{\mathbf{k},\mathbf{b}*}}{2i}) \right] & m \leq J', n \leq J', \\ -4 \sum_{\mathbf{b}} w_{\mathbf{b}} \left[\frac{R_{mn}^{\mathbf{k},\mathbf{b}*}}{2} + (1 - \lambda_c) \frac{T_{mn}^{\mathbf{k},\mathbf{b}*}}{2i} \right] - 4\lambda_c \sum_{\mathbf{b}} w_{\mathbf{b}} \left(\frac{\tilde{R}_{nm}^{\mathbf{k},\mathbf{b}*}}{2i} \text{Im} \ln M_{mm}^{\mathbf{k},\mathbf{b}} + \mathbf{b} \cdot \mathbf{r}_{0m} \frac{\tilde{R}_{nm}^{\mathbf{k},\mathbf{b}*}}{2i} \right) & m \leq J', n > J', \\ 4 \sum_{\mathbf{b}} w_{\mathbf{b}} \left[\frac{R_{mn}^{\mathbf{k},\mathbf{b}}}{2} - (1 - \lambda_c) \frac{T_{mn}^{\mathbf{k},\mathbf{b}}}{2i} \right] - 4\lambda_c \sum_{\mathbf{b}} w_{\mathbf{b}} \left(\frac{\tilde{R}_{mn}^{\mathbf{k},\mathbf{b}}}{2i} \text{Im} \ln M_{nn}^{\mathbf{k},\mathbf{b}} + \mathbf{b} \cdot \mathbf{r}_{0n} \frac{\tilde{R}_{mn}^{\mathbf{k},\mathbf{b}}}{2i} \right) & m > J', n \leq J', \\ 0 & m > J', n > J'. \end{cases} \end{aligned} \quad (35)$$

Minimizing this modified functional, we obtain Wannier functions that are maximally localized subject to the constraint of fixed centers. Although this constraint is satisfied at the cost of some delocalization, we can still maintain a high degree of localization through concurrent selective localization, as we illustrate in the applications below.

C. Fixing symmetry

It is further possible to ensure that the Wannier functions obtained preserve not only the desired centers, but also that they transform as irreducible representations of the point group, using for example the elegant group-theory-based approach recently introduced by Sakuma [6]. More straightforwardly one may simply introduce additional Lagrange multipliers, as discussed in Appendix A for the case of a one-dimensional model system. However, we have found that in all of the realistic examples studied in this paper orbitals which are localized to a site with a given point-group symmetry automatically transform as an irreducible representation of the respective point group. We do not presently have an analytical understanding of this empirical observation.

III. ONE-DIMENSIONAL CHAIN

To illustrate the utility of our method, we consider in this section a one-dimensional periodic lattice with δ potential barriers. In this system, there are an infinite number of isolated bands. As an example, we choose to construct a manifold of 4 Wannier functions (i.e., 4 bands) with 2 objective Wannier functions. We use a mesh with 100 k points for MLWF, SLWF, and SLWF+C. While considering examples in which symmetries are enforced (SLWF+CS), we use a mesh with 20 k points, due to the increased computational demands involved in those cases. In this one-dimensional problem, we study the following Hamiltonian:

$$H = -\frac{a^2}{2} \left(\frac{d}{dx} \right)^2 + \beta a \sum_j \delta(x - ja), \quad (36)$$

where a is the lattice constant and β is the dimensionless “strength” for the δ function. In practice, we choose $a = 5 \text{ \AA}$, $\beta = 0.6610$.

Figure 1(a) shows the Wannier functions resulting from MLWF (i.e., $J' = J = 4$). Three potential drawbacks are apparent. First, the MLWFs are nearly equally localized, which results in each MLWF having a relatively long tail. Second, we observe that none of the MLWFs are centered at either $x = 0$, the location of the periodic δ potential, or $x = 0.5a$, the midpoint between adjacent δ functions. Third, we notice that the MLWFs do not transform as irreducible representations of the order 2 point group at $x = 0$ or $x = 0.5a$.

Panel (b) of Fig. 1 shows the results of selective localization of two orbitals. Compared with MLWFs, the OWFs (solid red and green lines) become noticeably more localized [compare the tails of the functions in panels (a) and (b)]. The numerically computed spread $\langle (r - \langle r \rangle)^2 \rangle$ of the most localized MLWF is $0.2853a^2$ while the OWF has a spread of $0.0162a^2$. However, the remaining Wannier functions in the SLWF procedure, whose localization are ignored in the minimization procedure,

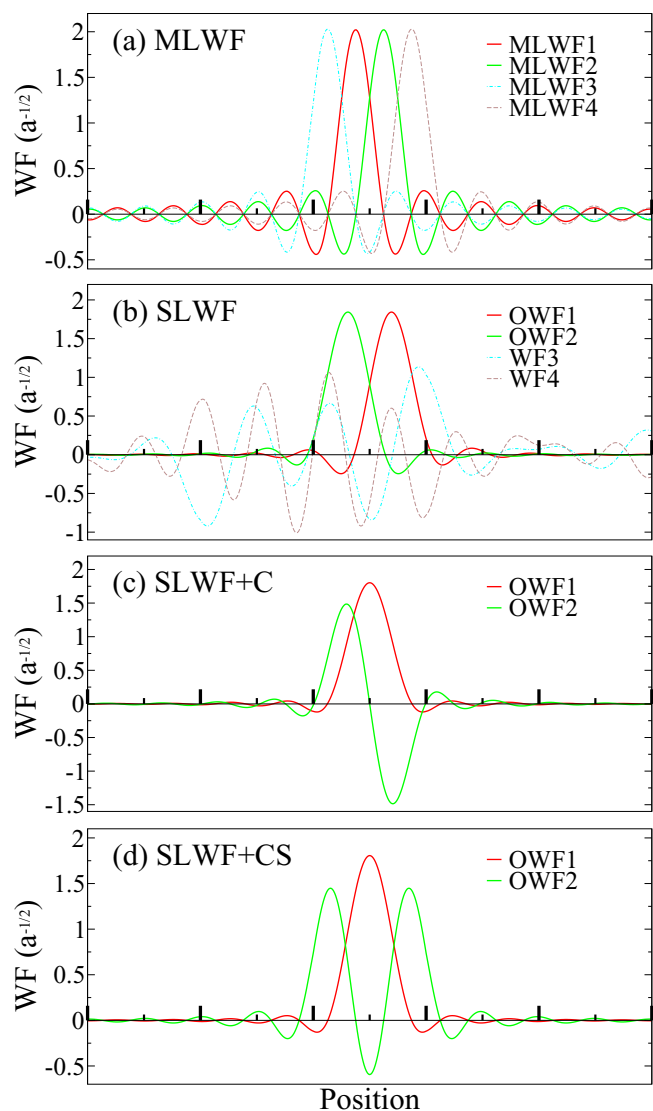


FIG. 1. (Color online) Wannier functions for the 1-d chain of δ -function potentials. Large tick marks denote the δ function, while small tick marks denote the midpoint. (a) MLWF for $J = J' = 4$. $\Omega_1 = \Omega_4 = 0.2853a^2, \Omega_2 = \Omega_3 = 0.2983a^2$. (b) SLWF for $J = 4, J' = 2$. $\Omega_1 = 0.0162a^2, \Omega_2 = 0.0162a^2$. (c) SLWF+C for $J = 4, J' = 2$. Both are located at $x = 0.5a$; $\Omega_1 = 0.0154a^2, \Omega_2 = 0.0605a^2$. (d) SLWF+CS for $J = 4, J' = 2$. Both are symmetric about $0.5a$; $\Omega_1 = 0.0154a^2, \Omega_2 = 0.1387a^2$.

become very delocalized. Using SLWF thus allows us to construct more localized objective Wannier functions at the expense of delocalization of the remaining ones.

Figure 1(c) presents the results obtained by fixing the centers of the two selectively localized orbitals to be at $x = 0.5a$. Fixing the centers increases the spread relative to the case where the centers were not constrained; however it is still much smaller than the summation of the two most localized MLWF spreads in the $J = J' = 4$ case. Furthermore, not only are the centers now located at the chosen sites, but the orbitals transform as the two possible irreducible representations (even and odd parity) of the order 2 group, respectively even though we have not forced the symmetry in any way.

In this one-dimensional chain, we can also introduce extra Lagrange multipliers to make the orbitals transform like particular irreducible representations, as outlined in Appendix A. For example, we force both objective Wannier functions to transform as the identity about $0.5a$ in the case $J = 4, J' = 2$ [see Fig. 1(d)]. The total spread has further increased relative to the previous case, with the spread of the second orbital nearly doubling, though now both orbitals are centered at $x = 0.5a$ and both transform as the identity representation of the order 2 group. Nonetheless, the largest spread of the OWF is still substantially less than the most compact MLWF. It should be noted that one must have a sufficient number of bands in the energy window to ensure that an arbitrary constraint can be fulfilled, and this issue is empirically addressed further in Appendix B. Further insightful examples in the one-dimensional chain are considered in Appendix B.

IV. APPLICATIONS

Having demonstrated the viability of our method in simple scenarios, we now turn to realistic applications involving relevant materials. Here we study GaAs, SrMnO₃, and Co, as they embody three different prototypical systems. In GaAs, we will show that our method produces atomic-like orbitals of appropriate local symmetry. SrMnO₃ is a prototypical transition-metal oxide with correlated electron properties, while in elemental Co the transition-metal d orbitals are not well separated from the less correlated s and p orbitals.

We use the Vienna *ab initio* Software Package (VASP) [7–10] to perform DFT calculations with projector augmented wave (PAW) potentials [11,12]. The exchange-correlation functional is treated within the generalized gradient approximation (GGA), as parametrized by Perdew, Burke, and Ernzerhof (PBE) [13]. In all calculations, we use experimental lattice constants, which are 5.653, 3.805, and 3.54 Å for GaAs, SrMnO₃, and Co, respectively. The mesh of k points is taken as $8 \times 8 \times 8$ with the Γ point included. Spin polarization is not included in the calculations. All the isosurface figures are plotted using the XCrySDen program [14].

While false local minima can in principle occur in our minimization procedure, they do not seem to occur in the applications presented in this section, as long as we start from reasonable trial projection functions.

A. GaAs

As shown in Ref. [2] for the zinc-blende GaAs, MLWF yields four identically localized Wannier functions (under T_d), exhibiting the character of sp^3 hybrids. Here, as a model to test our method, we construct the same number of Wannier functions but with only one objective Wannier function, and compare the results in 3 cases: (a) constructing four Wannier functions using MLWF with $J = 4, J' = 4$; (b) constructing four Wannier functions but using SLWF with $J = 4, J' = 1$; (c) constructing four Wannier functions using SLWF+C, fixing the center of the objective Wannier function to be at the position of As, with $J = 4, J' = 1$. In each case, the minimization is initialized with 4 trial s orbitals, centered in the middle of the bonds as the projection functions.

TABLE I. Minimized spreads in GaAs (units are Å²) from different methods. An asterisk * indicates the objective Wannier function constructed in the SLWF and SLWF+C method.

	MLWF	SLWF	SLWF+C
1*	2.1977	1.4283	1.4764
2	2.1977	3.0330	4.1243
3	2.1977	3.0330	4.1243
4	2.1977	3.0330	4.1243

Table I reports the spreads of all four Wannier functions in each method. As anticipated, SLWF makes the objective Wannier function (1*) most localized at the expense of the remaining Wannier functions. SLWF thus localizes the objective Wannier function at the cost of an increased total spread summed over all four Wannier functions. SLWF also pushes the Wannier center closer to the As ion. Following Ref. [2] we consider β , the ratio of the distance between the Wannier center and the Ga ion, and the length of the Ga-As bond. Using MLWF, we obtain $\beta = 0.618$, whereas using SLWF, we obtain $\beta = 0.706$. Of course, when we force the center to be located at the As site (SLWF+C), we have $\beta = 1$.

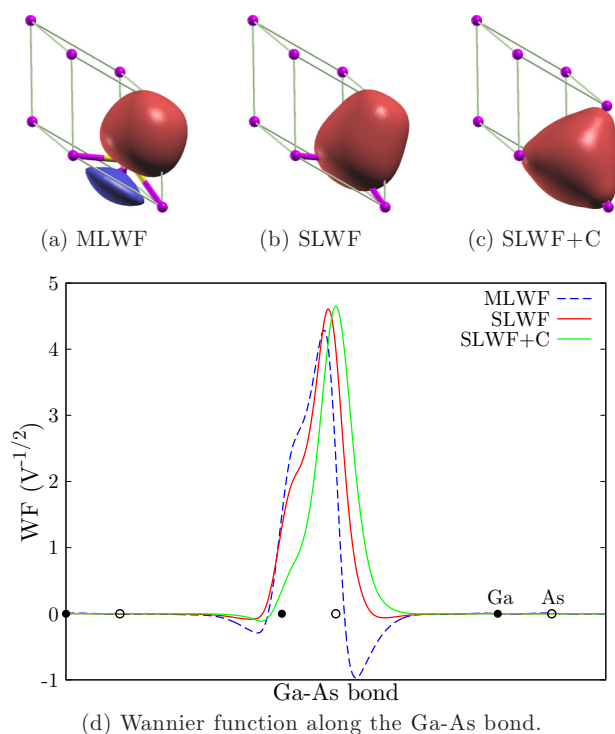


FIG. 2. (Color online) Wannier functions for GaAs obtained from different methods. In panels (a)–(c), Ga ions are indicated by purple spheres on the lattice corners; As ions are blocked from view by the Wannier function isosurfaces. The absolute value of the isosurfaces is $0.5/\sqrt{V}$, where V is the unit cell volume. Isosurfaces with positive amplitudes are colored red; those with negative amplitudes are colored blue. The Wannier functions are all real valued. Panel (d) shows a slice of each Wannier function along the Ga-As bond. The OWF function is plotted for the SLWF and SLWF+C methods.

TABLE II. Minimized spreads in SrMnO₃ and Co (units are Å²) obtained via MLWF and SLWF.

	SrMnO ₃		Co	
	MLWF	SLWF	MLWF	SLWF
$3z^2 - r^2$	0.5056	0.5006	0.5144	0.5051
xz	0.5486	0.5467	0.8505	0.5615
yz	0.5486	0.5467	0.8505	0.5615
$x^2 - y^2$	0.5056	0.5006	0.5144	0.5051
xy	0.5486	0.5467	0.8505	0.5615

In this case, fixing the center only causes a mild increase in the spread of the objective Wannier function.

In Fig. 2, we present plots showing the objective Wannier function obtained via the different methods. Interestingly, when we fix the center to locate at the position of As, the shape of the objective Wannier function naturally changes such that it transforms like the identity under T_d . Figure 2(d) further illustrates that SLWF smooths out the large bumps that arise in solutions obtained using MLWF.

In summary, we have demonstrated that SLWF has functionality that cannot be achieved using MLWF. However, these functionalities are not clearly relevant to the physics of GaAs; the results are thus a proof of principle.

B. SrMnO₃

We next turn to consider the Wannier functions corresponding to the d orbitals of Mn and p orbitals of O in the cubic perovskite SrMnO₃. In this material, there is an isolated manifold of 14 bands, which encompasses the Fermi energy. This manifold is predominantly composed of Mn d and oxygen p character (see Fig. 7). MLWF will localize all

14 Wannier functions weighted equally. However, the physics of this compound is driven by correlations on the d orbitals, so we seek a method which adequately localizes only these orbitals. We therefore apply our SLWF to localize 5 objective Wannier functions out of the total 14. We initialize using 5 trial d orbitals centered on Mn and 9 trial p orbitals centered on O as the projection functions.

In Table II, we compare the spreads of the 5 d -like MLWFs and the OWFs. Though the differences are very minimal, SLWF constructs d -like Wannier functions that are slightly more localized. In Fig. 3, we plot an isosurface of $0.1/\sqrt{V}$ for both cases, in which the Wannier functions transform like e_g and t_{2g} orbitals centered at the Mn site. Compared with the MLWFs, the OWFs show noticeably smaller tails. However, since the value of the isosurface in the plot is quite small, the differences are in fact very minimal. This feature is also apparent in the plot along the z axis for the $3z^2 - r^2$ -like MLWF and OWF shown in Fig. 4.

In summary, in the high-symmetry, separated-band case of SrMnO₃, our SLWF procedure has very minimal differences as compared to MLWF in terms of the spread for this test case. Further analysis will be performed in the next section where we analyze the Hamiltonian.

C. Co

The final example considered is Co, a transition metal in which the electronic structure is less ionic than a transition-metal oxide. Additionally, and unlike the cases considered in the previous two subsections, there is no clear separation between the highest retained bands and subsequent bands in the electronic structure. Specifically, we consider Co in the face-centered-cubic (fcc) structure, and we construct a set of 6 Wannier orbitals by including the lowest 6 bands, which encompasses the narrow d bands and free-electron-like s band

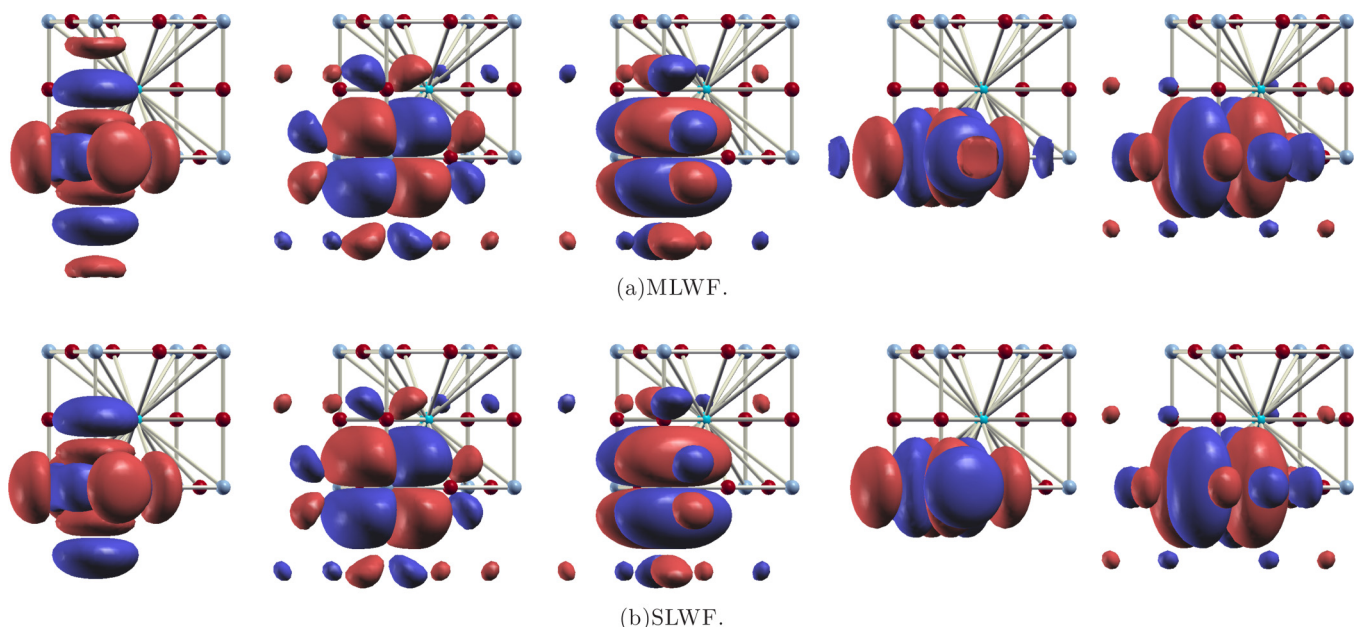


FIG. 3. (Color online) Comparison between the MLWF and SLWF method for SrMnO₃. Sr is the light blue sphere in the center, Mn is the blue sphere on the corner, O is the red sphere. In both panels, the 5 d -like Wannier functions are on the order of $3z^2 - r^2$, xz , yz , $x^2 - y^2$, xy , from left to right. The absolute value of the isosurfaces is $0.1/\sqrt{V}$.

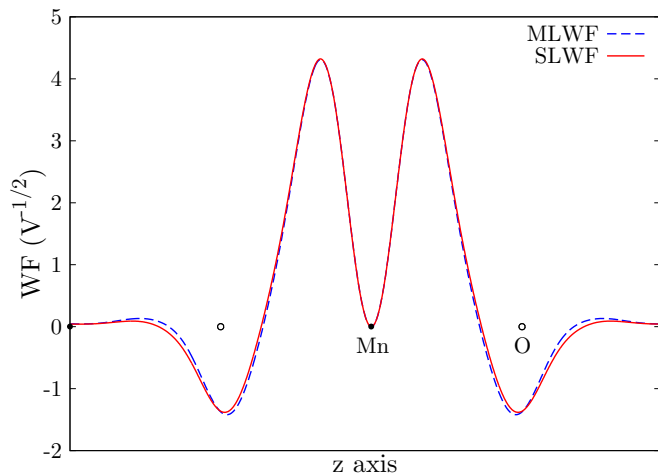


FIG. 4. (Color online) Wannier function along the z axis for the $3z^2 - r^2$ -like Wannier function generated from MLWF and SLWF in SrMnO_3 .

which hybridizes with the d bands. In our SLWF construction we choose 5 objective Wannier functions (i.e., $J = 6$ and $J' = 5$). We initialize both cases by using atom-centered trial d orbitals together with a trial s orbital which is centered around one of the tetrahedral-interstitial sites.

The right-hand column of Table II summarizes the spreads of the 5 d -like Wannier functions obtained using the two localization methods. As shown, SLWF decreases the spread relative to MLWF in all 5 orbitals, with strong decreases in the t_{2g} manifold. It is also worth noting that the OWFs we obtain using SLWF in Co are nearly as localized as in SrMnO_3 . In Fig. 5, we compare the isosurface plots of the d -like MLWFs and the OWFs. In the MLWF case we still use the same orbital labels for the three t_{2g} -like orbitals for simplicity although

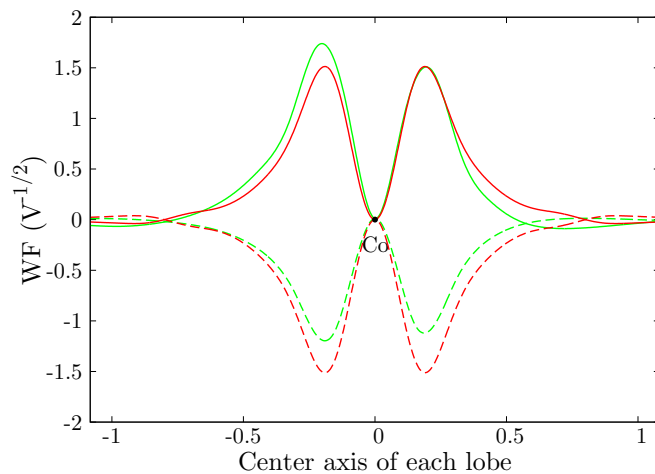


FIG. 6. (Color online) Wannier function along the center axis of each lobe for the xz -like Wannier function generated from MLWF and SLWF in Co. The light (green) lines represent MLWF while the dark (red) lines represent SLWF. For a given method, the solid lines are along the lobes with positive phase while the dashed lines are along the ones with negative phase. The horizontal axis is in units of the lattice constant.

the t_{2g} -like MLWFs have apparently lost t_{2g} symmetry and there are indications that the s orbital has been mixed in. In Fig. 6, we plot one of the t_{2g} -like MLWFs and OWFs along the center axis of each lobe, in units of the lattice constant. It is obvious that the 4 lobes in MLWF do not have the same shape any more while the OWF preserves the t_{2g} symmetry. Therefore, we conclude that SLWF offers improvements for creating atomic-like d orbitals for use in beyond-DFT methods in transition metals.

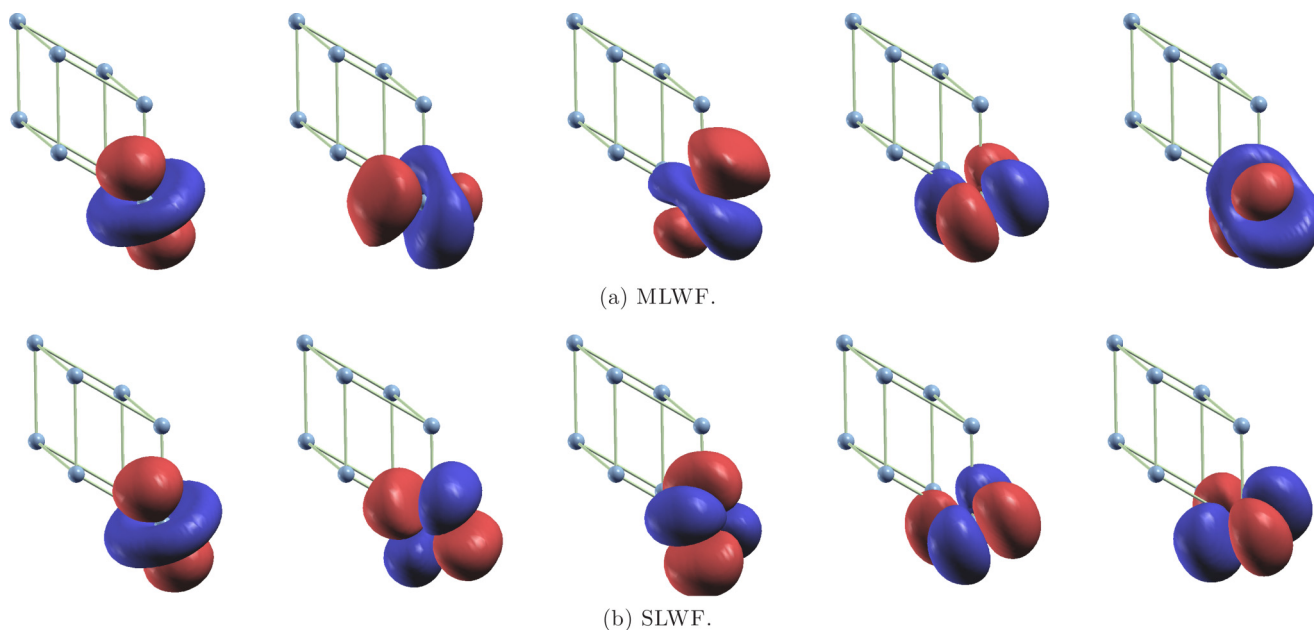


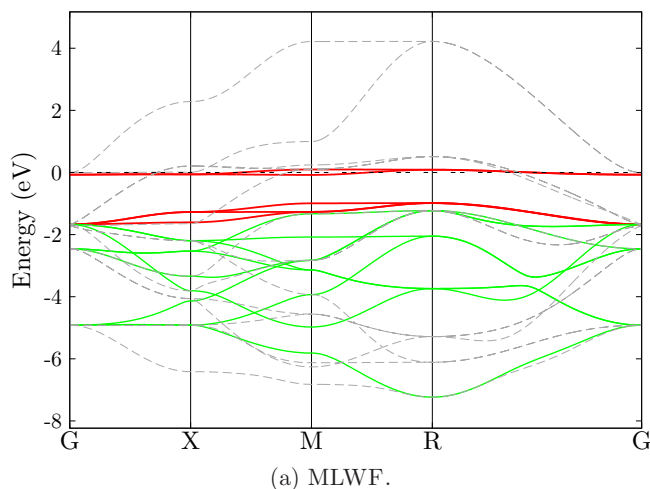
FIG. 5. (Color online) Comparison between the MLWF and SLWF method for Co. Co atoms are indicated by blue spheres on the lattice corners. In both panels, the 5 d -like Wannier functions are in the order of $3z^2 - r^2$, xz , yz , $x^2 - y^2$, xy , from left to right. The absolute value of the isosurfaces is $0.2/\sqrt{V}$.

V. HAMILTONIAN IN MLWF AND SLWF BASES

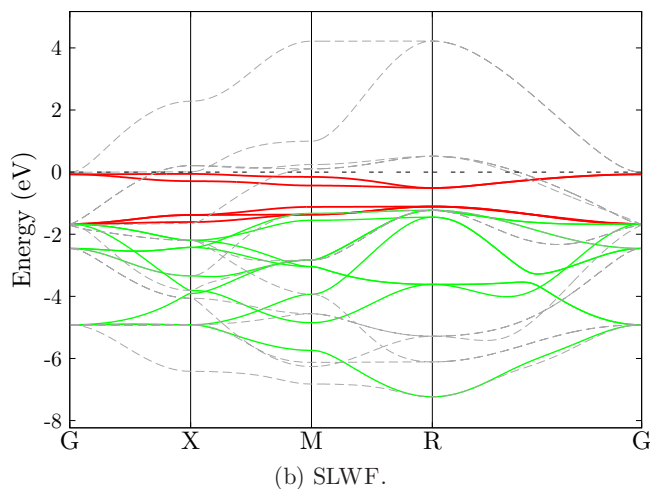
Thus far we have only examined the spatial properties of the Wannier orbitals, but another important aspect of the Wannier orbitals is the nature of the Hamiltonian in this basis. In order to elucidate this and to understand the differences in the Hamiltonians for MLWF and SLWF, we will follow the analysis put forward by Toropova *et al.* [15] in constructing Hamiltonians for SrMnO₃ and Co. In general we will have a k -space Hamiltonian with an objective orbital block and some other block of states that hybridizes with the objective block. In our test cases the objective orbitals correspond to a d block while the hybridizing orbital would be an s orbital for Co and p orbitals for SrMnO₃:

$$H(\mathbf{k}) = \begin{pmatrix} H_d(\mathbf{k}) & V(\mathbf{k}) \\ V^\dagger(\mathbf{k}) & H_{sp}(\mathbf{k}) \end{pmatrix}, \quad (37)$$

where the subscript sp simply denotes the block of orbitals that are not d . The effect of hopping within the d manifold versus hybridization can easily be seen in the “sliced” band structure. This simply amounts to zeroing $V(k)$ and then diagonalizing

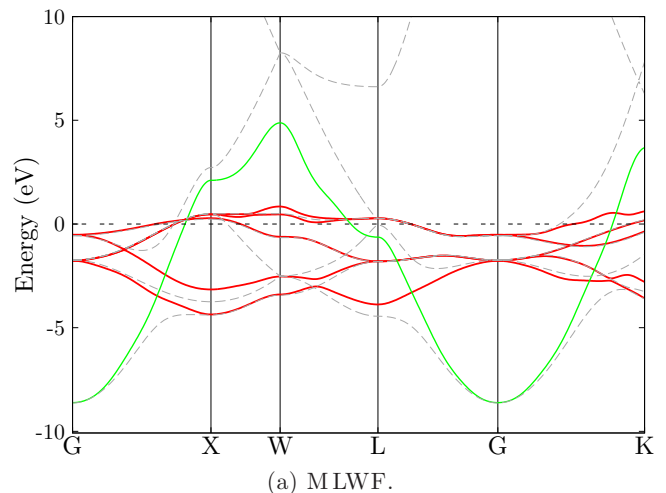


(a) MLWF.

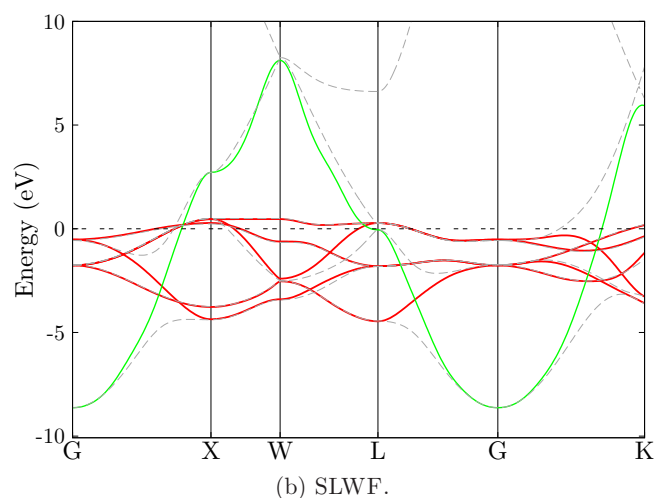


(b) SLWF.

FIG. 7. (Color online) Sliced band structures of SrMnO₃. In both panels, dashed gray lines represent the DFT band structure; solid dark (red) lines represent bands for the block H_d ; solid light (green) lines represent bands for the block H_p .



(a) MLWF.



(b) SLWF.

FIG. 8. (Color online) Sliced band structures of Co. In both panels, dashed gray lines represent the DFT band structure; solid dark (red) lines represent bands for the block H_d ; solid light (green) lines represent bands for the block H_s .

the separate blocks of the Hamiltonian at each k point, yielding a set of bands for each block. This allows one to see the bandwidth generated solely from hopping within the respective manifold, and the difference with the DFT band structure indicates the role of hybridization. We consider the case of SrMnO₃ and Co, following the exact same Wannier procedure as was outlined above.

In the case of SrMnO₃, we see that the d bands have several differences (see Fig. 7). The t_{2g} bands are narrower for SLWF, while the e_g bands are narrower for MLWF. The latter observation is particularly counterintuitive given that one clearly observes an enhanced localization of the objective e_g orbitals in Fig. 3. However, these differences are most likely not relevant for actual calculations.

In the case of Co, the differences between SLWF and MLWF are larger (see Fig. 8). In the case of MLWF, one can see that at the W point the s band is roughly 3 eV away from the DFT band, indicating a strong hybridization between the s -like and d -like MLWFs must be present. This is a symptom of the character mixture that we visually observed in Fig. 5 and quantified via the substantially larger spread of the

t_{2g} -like orbitals. In contrast, the s band obtained in the SLWF procedure nicely tracks the DFT band in the region of the W point. The complementary aspect of this result is that the sliced SLWF d bands more closely track the relevant DFT bands. The same points can be made near the K point. It appears clear in this case that the SLWF procedure results in a more appropriate set of d orbitals from the perspective of the Hamiltonian.

VI. CONCLUSIONS

We have generalized the algorithm introduced by Marzari and Vanderbilt [2] to allow for the maximal localization of a subset of Wannier functions, with fixed centers and symmetry. This scheme allows us to achieve greater localization for the selected subset of Wannier functions. We found that simply fixing the Wannier center produced orbitals that transformed as appropriate irreducible representations of the local point group even without specifying the symmetry.

We illustrated our method on GaAs, SrMnO₃, and Co. From the study of GaAs we demonstrate the power of our approach by constructing a single Wannier orbital which transforms like the identity, in addition to three delocalized orbitals which span the 4-band s - p manifold. In the case of SrMnO₃, we found that our SLWF procedure yielded results very similar to those found in the MLWF procedure, suggesting that MLWF may be sufficient for beyond-DFT calculations in transition-metal oxides. In the case of Co, SLWF offers notable improvements and results in a much purer set of d orbitals, which could be very important in the context of DFT+DMFT calculations. Future work should be performed explicitly comparing these two approaches in the context of DFT+DMFT. Implementing our approach within existing MLWF codes is straightforward.

ACKNOWLEDGMENTS

We thank Andreas Klöckner and Se Young Park for helpful discussions. A.J.M. was supported by DOE-ER046169. C.A.M., R.W., E.A.L., and H.P. were funded by NSF under

Contract No. DMR-1122594. This research used resources of the National Energy Research Scientific Computing Center, a DOE Office of Science User Facility supported by the Office of Science of the U.S. Department of Energy under Contract No. DE-AC02-05CH11231.

APPENDIX A: FIXING SYMMETRIES IN ONE DIMENSION

In this Appendix we show how we enforce symmetry constraints in one-dimensional systems. Assuming that the center of symmetry is at x_0 , the functional we want to minimize is

$$\Omega_s = \Omega_c + \lambda_s \sum_{n=1}^{J_s} \int_{-\infty}^{\infty} |(1 - \sigma_{x_0})w_n(x)|^2 dx + \lambda_s \sum_{n=J_s+1}^{J'} \int_{-\infty}^{\infty} |(1 + \sigma_{x_0})w_n(x)|^2 dx, \quad (\text{A1})$$

where J_s is the number of the objective Wannier functions we would like to be symmetric, while the other $J' - J_s$ would be antisymmetric; λ_s is a Lagrange multiplier for the corresponding constraint; σ_{x_0} is the mirror operator.

We define

$$I_{mn}^k = \frac{1}{N} \sum_{k'} \left[\int_{-\infty}^{\infty} \psi_{nk}(x) \sigma_{x_0} \psi_{mk'}^*(x) dx + \int_{-\infty}^{\infty} \psi_{mk'}^*(x) \sigma_{x_0} \psi_{nk}(x) dx \right]. \quad (\text{A2})$$

Under the infinitesimal unitary transformation, we have

$$d \left[\int_{-\infty}^{\infty} |(1 \pm \sigma_{x_0})w_n(x)|^2 dx \right] = \pm \frac{2}{N} \sum_k \sum_{m=1}^J \text{Re} (I_{nm}^k dW_{mn}^k). \quad (\text{A3})$$

Thus,

$$d\Omega_s = d\Omega_c - \lambda_s \frac{2}{N} \sum_k \left[\sum_{n=1}^{J_s} \sum_{m=1}^J \text{Re} (I_{nm}^k dW_{mn}^k) - \sum_{n=J_s+1}^{J'} \sum_{m=1}^J \text{Re} (I_{nm}^k dW_{mn}^k) \right]. \quad (\text{A4})$$

The gradient of Ω_s is then

$$G_{s,mn}^k = \frac{d\Omega_s}{dW_{mn}^k} = G_{c,mn}^k + \begin{cases} -\lambda_s (I_{mn}^k - I_{nm}^{k*}), & m \leq J_s, n \leq J_s, \\ -\lambda_s (I_{mn}^k + I_{nm}^{k*}), & m \leq J_s, J_s < n \leq J', \\ -\lambda_s I_{mn}^k, & m \leq J_s, n > J', \\ \lambda_s (I_{mn}^k + I_{nm}^{k*}), & J_s < m \leq J', n \leq J_s, \\ \lambda_s (I_{mn}^k - I_{nm}^{k*}), & J_s < m \leq J', J_s < n \leq J', \\ \lambda_s I_{mn}^k, & J_s < m \leq J', n > J', \\ \lambda_s I_{nm}^{k*}, & m > J', n \leq J_s, \\ -\lambda_s I_{nm}^{k*}, & m > J', J_s < n \leq J', \\ 0, & m > J', n > J'. \end{cases} \quad (\text{A5})$$

Using this method, we can ensure that the objective Wannier functions preserve arbitrary symmetries in a one-dimensional system in addition to maintaining fixed centers, all while maintaining a high degree of localization by performing selective localization.

APPENDIX B: ONE DIMENSIONAL CHAIN WITH ATTRACTIVE DELTA POTENTIAL

This Appendix presents results obtained for a one dimensional chain of δ function potentials with negative values, i.e., the system considered in Sec. III but with a change of sign in the potential. In this system a straightforward tight-binding picture would be based on orbitals similar to the isolated delta-function bound states. We show that the SLWF procedure can be used to recover this picture, creating OWF that transforms according to the irreducible representations of the Hamiltonian. We also demonstrate that the SLWF procedure can be used to generate states with symmetries not actually present in the Hamiltonian, provided that enough states are retained.

In our analysis, we will consider two bands under a variety of different scenarios. We begin by comparing MLWF ($J = 2, J' = 2$) with SLWF for the case of $J = 2, J' = 1$, and in Fig. 9(a) we plot the most localized MLWF and the objective Wannier function. In this case, both procedures naturally center the Wannier functions at the potential and both orbitals transform like the identity. As expected, the OWF has a smaller spread than the MLWF. In the second case, we perform SLWF+C for $J = 2, J' = 1$ [see Fig. 9(b)]. First we center the OWF at the midpoint of the bond, successfully obtaining a symmetric function, though with a larger spread than the OWF which naturally centered itself on the potential. Subsequently, we chose to center the OWF about a point 1/3 of the way between the potentials, and this results in a similar spread and the Wannier function is no longer symmetric about its center [see Fig. 9(b)]. If we perform SLWF+CS and attempt to enforce the OWF to be symmetric about its center, which is a symmetry that does not exist in the Hamiltonian, we were not successful (not shown). However, if we perform the same test using $J = 7, J' = 1$ [see Fig. 9(c)], there is much more freedom as we are only minimizing 1 out of 7 bands and a nearly symmetric function can be obtained. Finally, we repeat

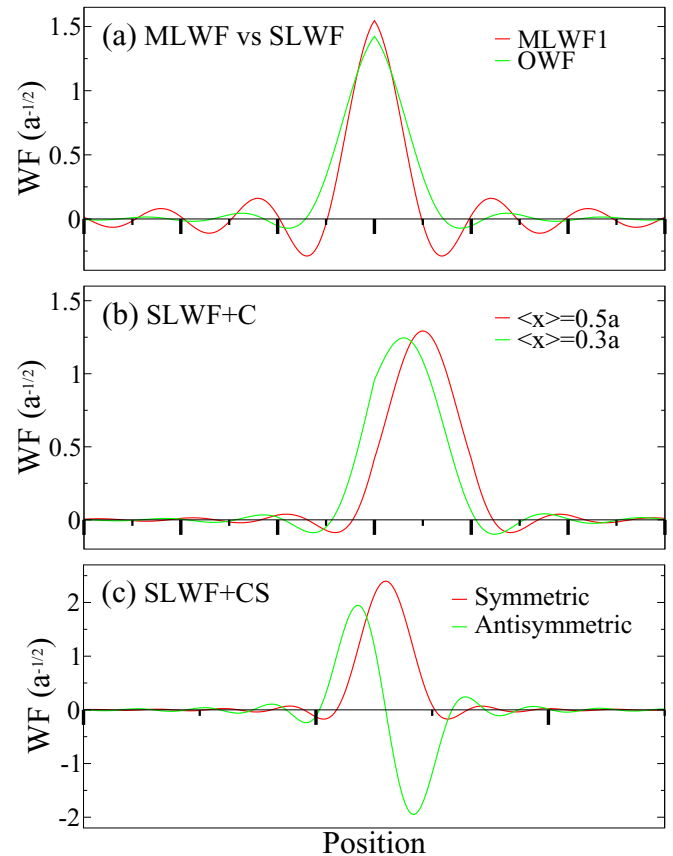


FIG. 9. (Color online) Wannier functions for the 1-d chain of negative δ -function potentials. Large tick marks denote the δ function, while small tick marks denote the midpoint. Panels (a) and (b) use 100 k points while panel (c) uses 20 k points. (a) Wannier functions obtained for $J = 2, J' = 2$ (MLWF), and $J = 2, J' = 1$ (SLWF). The spreads are $0.2713a^2$ and $0.0506a^2$, respectively. (b) OWF with centers fixed at $0.5a$ and $0.3a$ (SLWF+C), in the case of $J = 2, J' = 1$. The spreads are $0.0596a^2$ and $0.0637a^2$, respectively. (c) OWF with centers and symmetries controlled (SLWF+SC) in the case of $J = 7, J' = 1$. The spreads are $0.0050a^2$ and $0.0205a^2$ for symmetric OWF and antisymmetric OWF, respectively.

the preceding case but demand an antisymmetric function, demonstrating that this is straightforward.

[1] G. H. Wannier, *Phys. Rev.* **52**, 191 (1937).
 [2] N. Marzari and D. Vanderbilt, *Phys. Rev. B* **56**, 12847 (1997).
 [3] I. Souza, N. Marzari, and D. Vanderbilt, *Phys. Rev. B* **65**, 035109 (2001).
 [4] N. Marzari, A. A. Mostofi, J. R. Yates, I. Souza, and D. Vanderbilt, *Rev. Mod. Phys.* **84**, 1419 (2012).
 [5] A. Klöckner, Ph.D. thesis, Karlsruhe University, 2004.
 [6] R. Sakuma, *Phys. Rev. B* **87**, 235109 (2013).
 [7] G. Kresse and J. Hafner, *Phys. Rev. B* **47**, 558 (1993).

[8] G. Kresse and J. Hafner, *Phys. Rev. B* **49**, 14251 (1994).
 [9] G. Kresse and J. Furthmüller, *Comput. Mater. Sci.* **6**, 15 (1996).
 [10] G. Kresse and J. Furthmüller, *Phys. Rev. B* **54**, 11169 (1996).
 [11] P. E. Blöchl, *Phys. Rev. B* **50**, 17953 (1994).
 [12] G. Kresse and D. Joubert, *Phys. Rev. B* **59**, 1758 (1999).
 [13] J. P. Perdew, K. Burke, and M. Ernzerhof, *Phys. Rev. Lett.* **77**, 3865 (1996).
 [14] A. Kokalj, *Comput. Mater. Sci.* **28**, 155 (2003).
 [15] A. Toropova, C. A. Marianetti, K. Haule, and G. Kotliar, *Phys. Rev. B* **76**, 155126 (2007).